Title no. 92-S51

Splitting Bond Failure of Columns under Seismic Action

by Toshikatsu Ichinose

The mechanism of splitting bond failure in reinforced concrete columns subjected to reversed cyclic antisymmetric bending is analytically investigated. Reversed loading is found to accelerate bond failure in columns after flexural yielding because residual inelastic strains of longitudinal bars induced during opposite loading are forced in concrete. To prevent such failure, bond strength must be large enough to compress the residual strains. The necessary development length of bars running through a member with plastic hinges at its ends is presented.

Keywords: beams (supports); bonding; columns (supports); cyclic loads; ductility; energy.

The Japanese design guidelines for reinforced concrete buildings (Architectural Institute of Japan 1990) have a unique provision that neither ACI nor the CEB Code includes. This provision is intended to prevent splitting bond failure of continuous bars running through a member.

This failure has attracted the attention of Japanese researchers since the late 1970s, when they completed an experimental project on short columns of 260 specimens subjected to reversed cyclic antisymmetric bending. An example of the specimens is shown in Fig. 1 (Higashi and Ohkubo 1975), where the upper stub was pushed and pulled, keeping the upper stub parallel to the lower one. The project was motivated by the 1968 Tokachi-Oki earthquake and was intended to investigate shear failure before or after flexural yielding, but, in fact, about one-third of the specimens failed in splitting bond along longitudinal bars, even though the bars were well-anchored in stubs. Bond failure of the specimen in Fig. 1 is shown in Fig. 2. This failure mechanism reduces ductility and energy-dissipating capacity. The reduction is comparable to that of shear failure. During the 1983 Nihonkai-Chubu earthquake, many columns of Namioka Hospital failed in bond splitting, similar to Fig. 2 (Architectural Institute of Japan 1984).

The objectives of this paper are:

1. To investigate the mechanism of splitting bond failure in RC columns subjected to cyclic bending shear.
2. To propose a design criterion to prevent such failure.

The details of the analytical method used in this paper are shown in Appendix 1.* The method is essentially an extension of "plane sections" analysis, using uniaxial constitutive models of concrete, steel, and bond-slip. Equilibrium of moments and axial force are considered only at the two ends of a member. Equilibrium between longitudinal stresses of main bars and bond stresses is considered along the bars.

*The appendixes are available in xerographic or similar form from ACI headquarters, where they will be kept permanently on file, at a charge equal to the cost of reproduction plus handling at the time of request.

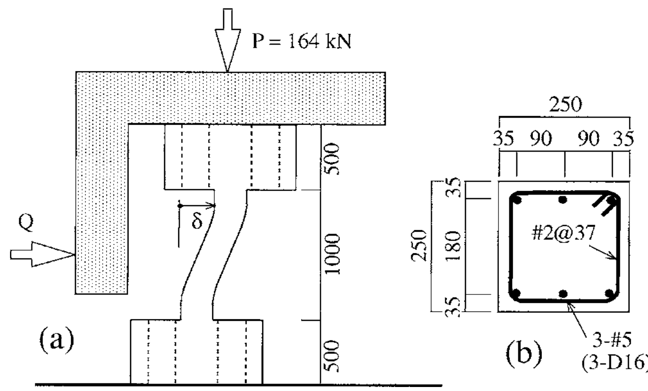

Fig. 1—Specimen LE-8B: (a) loading; and (b) section (1 mm = 0.039 in.).

RESEARCH SIGNIFICANCE

In 1971, ACI introduced the development length concept for anchorage, abandoning the requirement for flexural bond; the change simplified and rationalized anchorage design. This provision is now applied to terminating bars only. However, anchorage of continuous bars between critical sections of a member is also important for ductility and energy-dissipating capacity under reversed cyclic antisymmetric bending induced by seismic actions.

Splitting bond failure seldom occurs in cantilever-type specimens or specimens under monotonic antisymmetric bending, and, if any does occur, it seldom impairs ductility, as long as the two ends of the longitudinal bars are well-anchored. Thus, the splitting bond failure tends to be ignored.

The importance of bond failure is increasing because the strength of reinforcing bars and concrete is increasing, but it

ACI Structural Journal, V. 92, No. 5, September-October 1995.
Received April 11, 1994, and reviewed under Institute publication policies. Pertinent discussion will be published in the July-August 1996 *ACI Structural Journal* if received by March 1, 1996.

*ACI member **Toshikatsu Ichinose** is an associate professor of architecture at Nagoya Institute of Technology, Japan. He received his degrees from the University of Tokyo. His current research interests are shear, bond, and confinement of reinforced concrete. He was a member of the working group in charge of the shear and bond provisions in the 1990 Japanese Design Guidelines for Earthquake-Resistant Reinforced Concrete Buildings Based on Ultimate Strength Concept.*

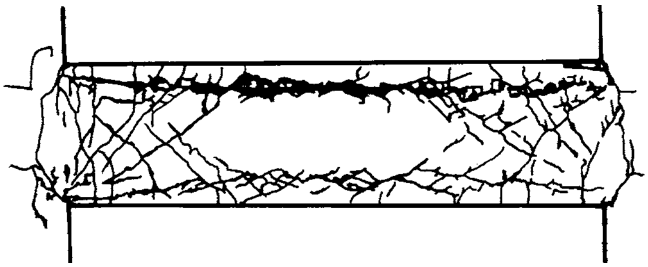

Fig. 2—Bond failure of Specimen LE-8B.

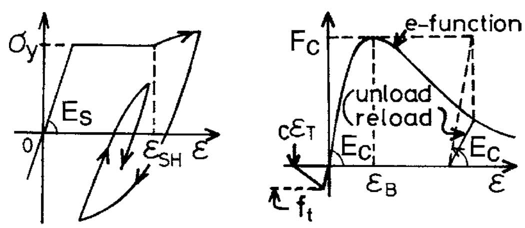

(a) (b)

Fig. 3—Stress-strain model: (a) steel; and (b) concrete.

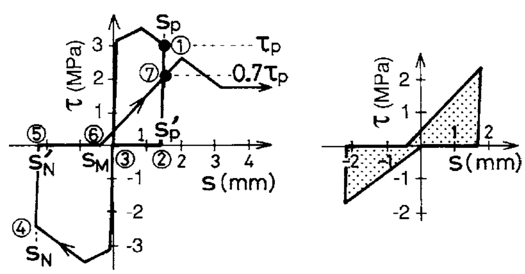

(a) (b)

Fig. 4—Bond slip model: (a) loading, unloading, and reloading; (b) stable loop (1 MPa = 1.45 ksi, 1 mm = 0.039 in.).

is not proportional to bond strength. Structural designers in seismic areas should pay attention to this failure, which may occur in severe earthquakes. This paper explains its mechanism and presents a way to prevent it.

MECHANISM OF BOND FAILURE UNDER CYCLIC LOADING

Higashi and Ohkubo (1975) prepared two identical specimens, whose dimensions are shown in Fig. 1. One of the specimens was loaded monotonically, i.e., the upper stub was only pushed. The other was loaded cyclically, i.e., the upper stub was pushed and pulled at various amplitudes of δ. Both of these specimens will be analyzed. The failure pattern shown in Fig. 2 was the cyclically-loaded specimen. Tensile reinforcement ratio of the specimens is 0.95 percent. Reinforcing steel is modeled as shown in Fig. 3(a), according to Fujii et al. (1973). Yield strength σ_y is 455 MPa (66 ksi). Strain at the onset of strain hardening ε_{sh} is 0.0174. Concrete is modeled as shown in Fig. 3(b), according to Okada et al. (1977). Compressive strength F_c is 24 MPa (3.5 ksi). Strain at that strength ε_B is 0.0019. Bond is modeled as shown in Fig. 4, according to Morita et al. (1975). Numbers 1 through 7 show the process of unloading and reloading. The unloading stiffness (1 to 2) is equal to the initial stiffness. Reloading point 6 is located at the middle of points 2 and 5, i.e. $s_M = (s_P' + s_N')/2$, if $|s_N'| > s_p'$. If $|s_N'| \le s_P'$, $s_M = 0$. When slip is repeated cyclically between s_P and s_N, the model makes a stable loop, as shown in Fig. 4(b). The envelope curve of the model is calculated according to the empirical equations of Fujii et al. (1982), considering spacing of main bars and amount of shear reinforcement. Bond strength near critical sections is reduced, considering flexural shear cracks; the detail of the reduction is shown in Appendix 2†. Pullout and push-in of longitudinal reinforcement from stubs are ignored.

Analytical shear-force deflection relationships of the specimens are plotted in Fig. 5(a), where the solid and broken lines show the results of cyclic and monotonic loading, respectively. Note that the envelope curve of cyclic loading is lower than that of monotonic loading. The circles and crosses show the loading steps when the slip at the center of the span reached s_2 and s_3 and the slips at the second (maximum) and third (final) breaking points of the bond slip envelope, respectively. In the cyclic analysis, the circle appears during the cycle of δ = 20 mm (0.8 in.), whereas in the monotonic analysis, it appears at δ = 36 mm (1.4 in.). The experimental results are partly plotted in Fig. 5(b) by dotted lines that agree with the analyses, including the shape of the hysteresis curve of the second cycle.

Fig. 5(c) shows the relationship between the deflection of the member and the stress of the longitudinal bar at the critical section first subjected to tension. Fig. 5(d) shows the relation subjected to compression first, where the compressive stress is taken to be positive. The upper half of Fig. 5(c) is similar to that of Fig. 5(a); the lower half of Fig. 5(d) is similar to that of Fig. 5(a). In other words, the shear-force is proportional to the tensile stress of the longitudinal bars at critical sections. However, the compressive stress of the bars is quite different from the shear-force deflection relationship. The compressive stress under cyclic loading is larger than that under monotonic loading, due to the residual tensile strain of the longitudinal reinforcement induced during the previous loading [see the stress-strain model for steel, Fig. 3(a)], where the steel carries compressive yield strength while the strain is still in tension. Such a tendency was first noted in the plane section analyses by Aoyama (1964). This large compressive stress in reversed loading requires larger bond stress between critical sections than in monotonic loading.

In Fig. 5(c) and 5(d), the compressive stress decreases from around δ = 10 mm (0.4 in.) because the bond strength is limited: as the tensile stress increases on one side, the compressive stress must decrease on the other side.

†The appendixes are available in xerographic or similar form from ACI headquarters, where they will be kept permanently on file, at a charge equal to the cost of reproduction plus handling at the time of request.

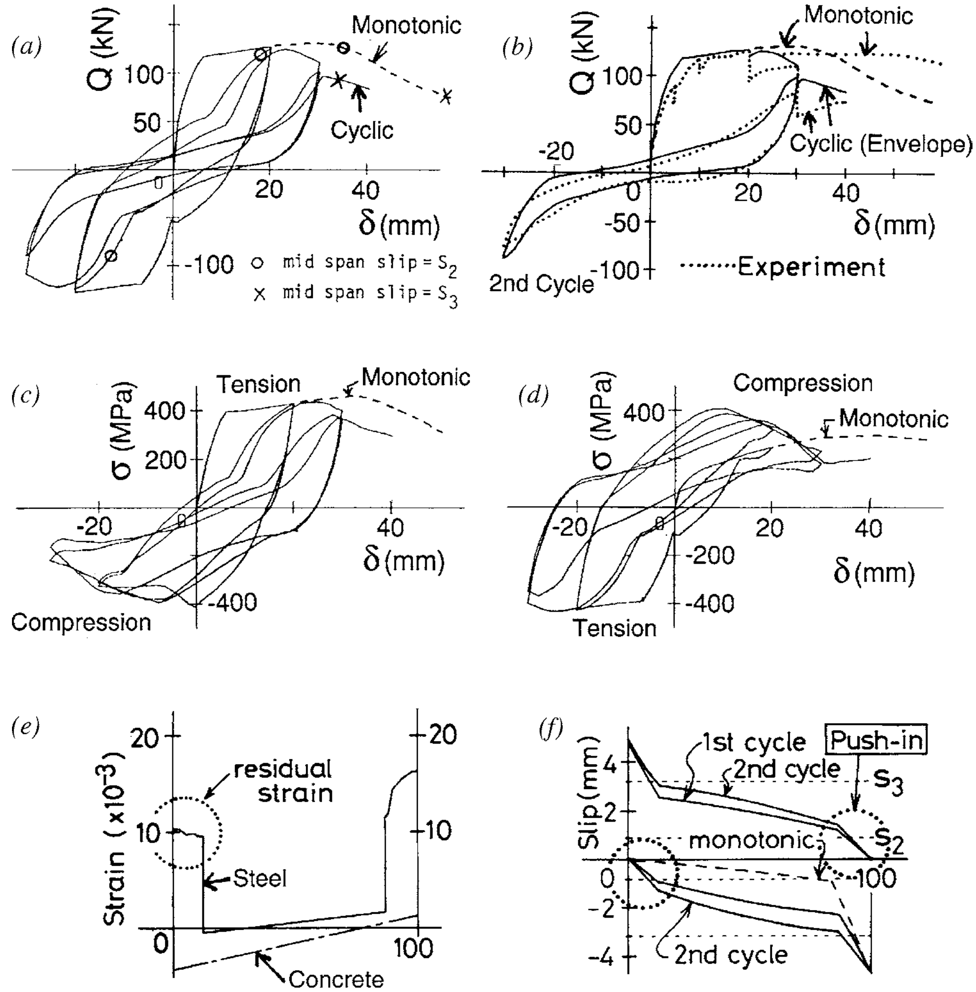

Fig. 5—Analytical results of LE-8B: (a) shear-force deflection relationship; (b) comparison with experiment; (c) steel stress at critical section (positive in tension); (d) steel stress at critical section (positive in compression); (e) distribution of strain at δ = 30 mm, second cycle; and (f) distribution of slip at δ = 30 mm (1 kN = 0.22 kip, 1 MPa = 1.45 ksi, 1 mm = 0.039 in.).

The distribution of the strains is shown in Fig. 5(e), where the solid and chained lines indicate the strains of steel and concrete along the main bars. The distribution of slips at $\delta = \pm 30$ mm (1.2 in.) is shown in Fig. 5(f), where the broken and solid lines represent slips during monotonic and cyclic loadings, respectively. The slip during the cyclic loading is much larger than in the monotonic loading, due to residual strains marked by the dotted circles in Fig. 5(e), where stresses are in compression but strains are in tension. These strains are pushed into the intermediate portion of the member, resulting in a large slip. This is why a member subjected to cyclic loading and failing in bond splitting has less ductility than one subjected to monotonic loading.

DEFINITION OF NORMALIZED BOND STRENGTH

In this paper, the effective bond strength τ_e is defined as

$$\tau_e = \frac{\tau_1 + \tau_2}{2} \tag{1}$$

where τ_1 and τ_2 are bond stresses at the first and second breaking points of the τ-s bond slip model. Fig. 6 shows a possible criterion for preventing bond failure in members subjected to reversed inelastic antisymmetric bending: effective bond strength τ_e must be large enough to sustain tensile and compressive yield strengths $\pm\sigma_y$ at the end of effective anchorage length Z, defined later. In other words,

$$\psi \tau_e Z \geq 2A\sigma_y \tag{2}$$

where ψ, A, and σ_y are the perimeter, cross-sectional area, and yield strength of the longitudinal bar, respectively. The effective anchorage length Z is defined as

$$Z = \ell - max(a_p, d) - a_N \tag{3}$$

where ℓ is the total length of the member; a_P and a_N are the plastic zone lengths induced during positive and negative loadings, calculated later; and d is the effective depth of the section. a_N is subtracted from ℓ because the stress must be larger than σ_y in the plastic zones to compress the residual

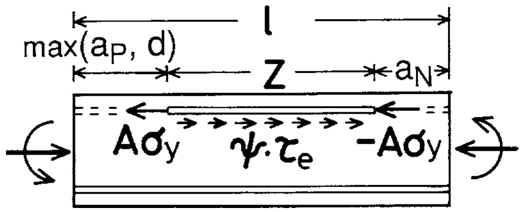

Fig. 6—Assumed criteria to prevent bond failure.

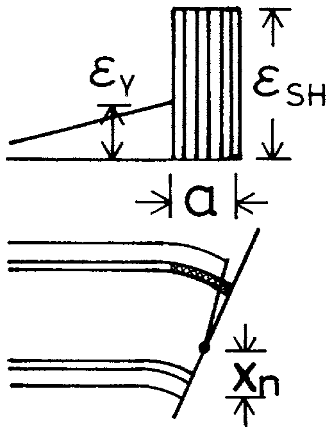

Fig. 7—Strain in plastic zone.

strains produced during negative loading. max(a_P, d) is subtracted from ℓ because bond strength is limited in tension sides of the member ends due to flexural shear cracks (see Fig. 6A in Appendix).

Noting $A/\psi = d_b/4$ (d_b: bar diameter), Eq. (2) is rewritten as

$$\alpha = \frac{2\tau_e Z}{\sigma_y d_b} \geq 1.0 \quad (4)$$

α will be called normalized bond strength. In terms of development length ℓ_d, Eq. (4) can be rewritten as

$$l_d = \frac{\sigma_y d_b}{4\tau_e} \leq \frac{Z}{2} \quad (5)$$

In calculating plastic zone lengths a_P and a_N, we will consider the case that deflection angles in positive and negative loadings are the same. Then, we may assume

$$a = a_p = a_N \quad (6)$$

In addition, the following will be assumed:

1. Pullout of longitudinal bars from neighboring beam-column joints is zero.
2. As shown in Fig. 7, strain in the plastic zone is uniformly ε_{SH}, the strain at the onset of strain hardening.
3. The depth of neutral axis x_n in Fig. 7 remains equal to that at flexural yielding and is given by plane section analyses.
4. Yield curvature κ_y is given by plane section analyses.

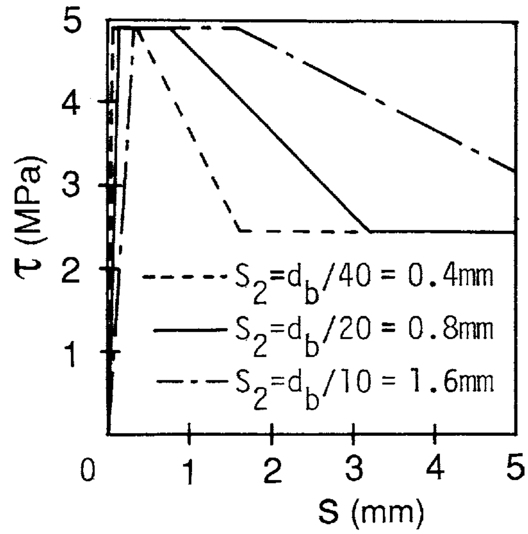

Fig. 8—Bond slip (τ-s) model for α = 1.0 (1 MPa = 1.45 ksi, 1 mm = 0.039 in.)

5. Yield deflection angle R_y is given as follows, assuming linear distribution of curvature

$$R_y = \frac{\kappa_y l}{6} \quad (7)$$

6. Elongation in the plastic zone, $a.\varepsilon_{SH}$, is equal to that induced by plastic rotation, $(R - R_y)(d - x_n)$. Thus, we have

$$a = \frac{(R - R_y)(d - x_n)}{\varepsilon_{SH}} \quad (8)$$

EFFECTS OF BOND STRENGTH AND DUCTILITY

According to Fujii and Morita (1982), lateral reinforcement increases the capacity to maintain bond stress after slip. This effect is known as bond ductility. This section examines whether $\alpha \geq 1$ can be a unique criterion for preventing bond failure or if bond ductility has any effect on the behavior of columns. We will use Specimen LE-8B in Fig. 1 again, and assume cyclic loading at deflection angle of R = 1/50 radian. Then, the criterion of $\alpha \geq 1$ requires bond strength of $\tau_e \geq 4.9$ MPa (0.7 ksi). The solid line in Fig. 8 shows a τ-s model satisfying $\alpha = 1$, where $s_1 = d_b/100$ (d_b: diameter of longitudinal bar), $s_2 = d_b/20$, and $s_3 = d_b/5$. The broken and chained lines in Fig. 8 are variations of the solid line: s_1, s_2, and s_3 are halved and doubled, respectively. According to Fujii and Morita (1982), the assumed s_2 of the broken and chained lines corresponds to p_w = 0.03 and 1.54 percent, representing the smallest and largest possible bond ductilities, respectively. The other parameter is the bond strength. In addition to $\alpha = 1$ in Fig. 8, we will analyze the cases of α = 0.8, 0.6, 0.4, 0.2 and 0, reducing τ_3 proportionally.

Examples of force-deflection relationships are shown in Fig. 9. In the case of no bond ($\alpha = 0$), the strength is only about 40 percent of the yield strength, and the energy dissipation in the second and third cycles is zero. In the case of α = 0.6 and $s_2 = d_b/40$, the cyclic loops shrink, and strength

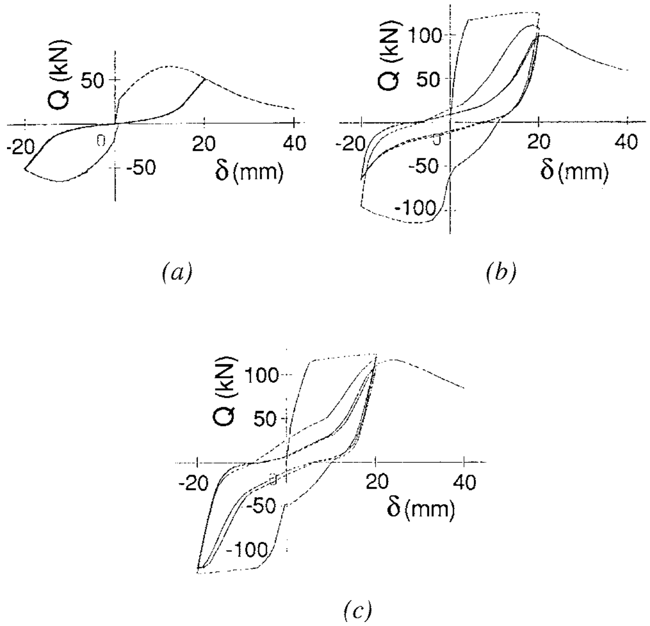

Fig. 9—Examples of force-deflection relationship: (a) α = 0; (b) α = 0.6 and $s_2 = d_b/40$*; (c) α = 0.6 and* $s_2 = d_b/10$ *(1 kN = 0.22 kip, 1 mm = 0.039 in.).*

degradation in the second and third cycles is large. In the case of α = 0.6 and $s_2 = d_b/10$, the cyclic loops shrink, but strength degradation is small.

The plastic zone length due to positive loading is shown in Fig. 10. Where α = 0 and 0.2, yielding does not occur. Eq. (6) gives a = 144 mm (5.7 in.), which approximates the results of α = 1. Compared with the total length of the member [1000 mm (39 in.)], this is not negligible.

The dissipated energy during the first and third cycles is shown in Fig. 11. The effect of bond ductility is smaller than bond strength. Dissipated energy during the first cycle increases in the range of α = 0 and 0.6, whereas during the third cycle, it increases to α = 0.6 and 1.

Load resistances at the first positive and third negative peak deflections are shown in Fig. 12. On the negative side of α = 0.6 and 0.8, the effect of bond ductility is large. At α = 1, load resistance exceeds yield strength Q_y, irrespective of bond ductility.

Slip at the center of span is shown in Fig. 13. Slip in the negative loading of α = 0.6 and $s_2 = d_b/40$ is larger than those in the other cases because yielding occurs in positive loading only, resulting in large push-in. At α = 1, slip is less than 0.4 mm (0.02 in.), irrespective of bond ductility. Slip causes pinching of the hysteresis loop. Since $(d - x_n)$ is about 170 mm (6.7 in.), slip of approximately 0.4 mm causes pinching of 0.4/170 = 1/400 radian, which is sufficiently small.

Analyses of columns with different axial force and reinforcement showed similar results, including the case of zero axial force (i.e., analyses of beams). We may, therefore, conclude that α ≥ 1 is the necessary and sufficient criterion for preventing bond failure after reversed cyclic loading. It guarantees small slip, resulting in large energy dissipation and load resistance.

As shown in Eq. (5), the criterion α ≥ 1 means that the development length of the main bars ℓ_d must be smaller than

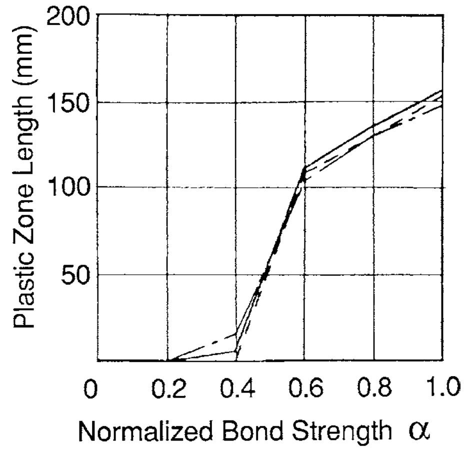

Fig. 10—Plastic zone length (1 mm = 0.039 in.).

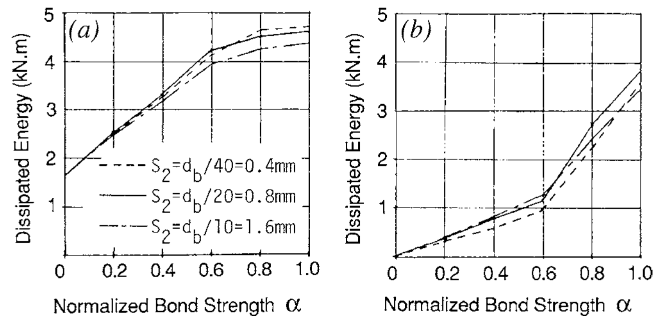

Fig. 11—Dissipated energy: (a) first cycle; (b) third cycle (1 kN.m = 8.8 in.-k).

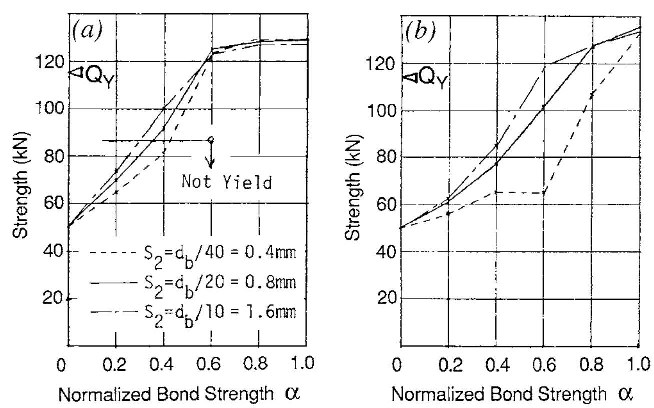

Fig. 12—Load at peak deflection: (a) first cycle, positive; (b) third cycle, negative (1 kN = 0.22 kip).

$Z/2$. If a member with a depth of neutral axis of $x_n = 0.2\,d$ is expected to evade bond failure under inelastic deflection angle $(R - R_y)$ = 1/100 radian, and the strain at the onset of strain hardening of the main bar is 0.02, then the plastic zone length a will be about $0.4d$ [see Eq. (8)]. Thus, $Z/2$ will be about $(\ell/2 - 0.7d)$. The coefficient 0.7 should be larger if the member is required to have a large ductility or the bar has a small yield plateau, since Eq. (8) has R in the numerator and ε_{sh} in the denominator.

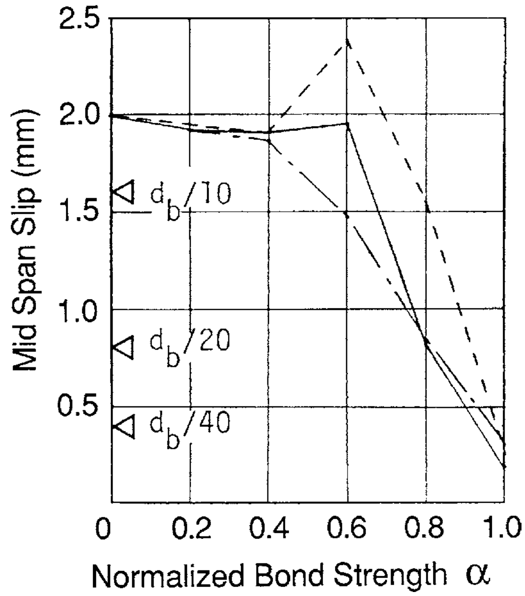

Fig. 13—Slip at center of span, negative peak of third cycle (1 mm = 0.039 in.).

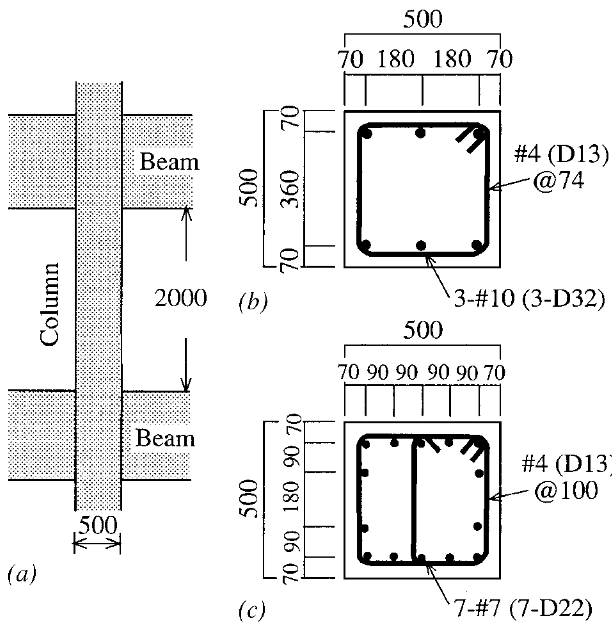

Fig. 14—Design example: (a) column in a frame; (b) original section; (c) revised section (1 mm = 0.039 in.).

DESIGN EXAMPLE

The specimen in Fig. 1 is used as a design example. Considering that the specimen was about one-half the model of a real column, we simply double the dimensions, as shown in Fig. 14(a) and (b). This is a column in an exterior frame shortened by spandrel beams. According to the previous discussion, the development length must be shorter than ($\ell/2 - 0.7d$) = 2000/2 – 0.7 × 430 = 785 mm (31 in.). According to ACI metric provisions

$$\ell_d = 0.02A\sigma_y/\sqrt{F_c} = 0.02 \cdot 794 \cdot 455/\sqrt{24} \quad (9)$$

$$= 1475 \text{ mm (58 in.)}$$

This is too long. Let us modify the section, as shown in Fig. 14(b), which has flexural and shear strengths similar to those in Fig. 14(a). This section gives

$$\ell_d = 0.02A\sigma_y/\sqrt{F_c} = 0.02 \cdot 387 \cdot 455/\sqrt{24} \quad (10)$$

$$= 719 \text{ mm (28 in.)}$$

which is larger than 785 mm (31 in.) and is acceptable. Japanese design guidelines (1990) give a similar result.

CONCLUSIONS

1. Reversed cyclic loading accelerates bond failure in columns because residual inelastic strains induced during opposite loading are forced into concrete. This is the reason a member subjected to cyclic loading and failing in bond splitting has less ductility than one subjected to monotonic loading. To prevent such failure, bond strength must be large enough to compress residual strains.

2. Main bars running through a ductile column or beam with hinge regions at its two ends should satisfy a provision that its development length must be smaller than about ($\ell/2 - 0.7d$), where ℓ and d are the total length and the effective depth of the member, respectively. Coefficient 0.7 should be larger if the member is required to have a large ductility or the bars have small yield plateau.

ACKNOWLEDGMENTS

Grateful thanks to Professor Emeritus Hiroyuki Aoyama and Professor Shunsuke Otani of the University of Tokyo for their kind guidance and valuable suggestions.

NOTATION

A	=	cross-sectional area of longitudinal bar
a_P	=	plastic zone lengths induced during positive and negative loadings
a_N	=	plastic zone lengths induced during positive and negative loadings
d	=	effective depth of section
d_b	=	diameter of longitudinal bar
F_c	=	compressive strength
ℓ_d	=	development length
ℓ	=	total length of member
R_y	=	deflection angle of member at yielding of longitudinal bars
s_1	=	slip at first breaking point of bond slip model
s_2	=	slip at second breaking point of bond slip model
s_3	=	slip at third breaking point of bond slip model
s_N	=	maximum positive and negative slip
s_N'	=	slip at reloading point from s_P and s_N
s_P	=	maximum positive and negative slip
s_P'	=	slip at reloading point from s_P and s_N
x_n	=	depth of neutral axis
Z	=	effective anchorage length defined by Eq. (3)
α	=	normalized bond strength defined by Eq. (4)
δ	=	deflection of member
ε_B	=	strain of concrete at compressive strength
ε_{sh}	=	strain at onset of strain hardening
κ_y	=	curvature of section at yielding of longitudinal bars
σ_y	=	yield strength of reinforcing bar
ψ	=	perimeter of longitudinal bar
τ_e	=	effective bond strength (average of τ_1 and τ_2)
τ_1	=	bond stress at first breaking point of bond slip model
τ_2	=	bond stress at second breaking point of bond slip model
τ_p	=	bond stress at s_P

REFERENCES

ACI Committee 318, 1989, "Building Code Requirements for Reinforced Concrete (ACI 318-89) and Commentary (318R-89), American Concrete Institute, Detroit, 353 pp.

Aoyama, H., 1964, "Moment-Curvature Characteristics of RC Members Subjected to Axial and Reversal of Bending," *Proceedings of International Symposium on Flexural Mechanics of Reinforced Concrete*, ASCE-ACI, Miami, pp. 183-212.

Architectural Institute of Japan, 1984. *Report on the Damage Investigation of Urakawa-Oki Earthquake 1982 and Nihonkai-Chubu Earthquake 1983*, 435 pp. (in Japanese)

Architectural Institute of Japan, 1990. *Design Guidelines for Earthquake-Resistant Reinforced Concrete Buildings Based on Ultimate Strength Concept*, 340 pp. (in Japanese; English version published in 1994)

Fujii, S.; Aoyama, H.; and Umemura, H., 1973. "Moment-Curvature Relationship of RC Sections Based on Material Characteristics," *Annual Meeting of Architectural Institute of Japan*, pp. 1261-1262. (in Japanese)

Higashi, Y.; Ohkubo, Z.; and Ohtsuka, M., 1975. "Comprehensive Study on the Prevention of Failure of Reinforced Concrete Columns," *Annual Meeting of Architectural Institute of Japan*, pp. 1113-1116. (in Japanese)

Ichinose, T., 1986. "Bond Slip in Reinforced Concrete Beam-Column Joint," *Transactions of Architectural Institute of Japan*, No. 367, pp. 151-159. (in Japanese)

Morita, S., and Fujii, S., 1982. "Bond Capacity of Deformed Bars Due to Splitting of Surrounding Concrete," *Bond in Concrete*, P. Bartos, ed., Applied Science Publishers, pp. 331-341.

Morita, S., and Kaku, T., 1975. "Study on Bond Characteristics between Steel and Concrete under Cyclic Loading," *Transactions of Architectural Institute of Japan*, No. 229, pp. 15-24. (in Japanese)

Okada, T.; Seki, M.; Asai, T.; Park, E.; and Okada, T., 1977. "Response of RC Buildings Subjected to Bidirectional Seismic Loading—Part 1," *Annual Meeting of Architectural Institute of Japan*, pp. 1881-1882. (in Japanese)

92-S51

Supplement to:

ACI STRUCTURAL JOURNAL

Appendix to:

Title no. 92-S51 , *ACI Structural Journal*, V. 92, No. 5, September-October 1995, pp. 535-542

"Splitting Bond Failure of Columns under Seismic Action" by T. Ichinose

G:\wpdata\data\journal.frm\append.str

Appendix 1 : ANALYTICAL METHOD

Definitions

Inner forces and deformations of a member are defined in Fig. A1. The inner force vector **f** is composed of the bending moments and the axial forces at the member ends as follows.

$$\mathbf{f} = \{M_A, N_A, M_B, N_B\}^t \tag{A1}$$

The deformation vector **d** is defined by the following equations integrating the curvature κ and the axial strain ε_o of the member, whose rigorous definition will appear later.

$$\mathbf{d} = \{\theta_A, e_A, \theta_B, e_B\}^t \tag{A2}$$

$$\theta_A = -\int_0^\ell (1-\frac{x}{\ell})\kappa \cdot dx \tag{A3}$$

$$e_A = -\int_0^\ell (1-\frac{x}{\ell})\varepsilon_o \cdot dx \tag{A4}$$

$$\theta_B = \int_0^\ell \frac{x}{\ell} \cdot \kappa \cdot dx \tag{A5}$$

$$e_B = \int_0^\ell \frac{x}{\ell} \cdot \varepsilon_o \cdot dx \tag{A6}$$

where θ_A and θ_B are the rotation angles of the member shown in Fig. A1; e_A and e_B are the horizontal displacements of the member ends measured from the point where the horizontal displacement is average (see the vertical roller shown in Fig. A1).

Assumptions

The following eight assumptions are made for the analysis:

(1) Equilibrium between longitudinal stresses of main bars and bond stresses is considered along main bars as shown in Fig. A2, where A, σ_s, ψ, τ are sectional area, longitudinal stress, perimeter, bond stress of main bar, respectively.

$$A\frac{d\sigma_s}{dx} = \psi . \tau \tag{A7}$$

(2) Compatibility among slip, steel strain and concrete strain is considered along main bars as in the following equation, where s, ε_s, ε_c are slip, steel strain and concrete strain, respectively.

$$\frac{ds}{dx} = \varepsilon_s - \varepsilon_c \tag{A8}$$

(3) Equilibrium of moments and axial forces induced by stresses of steel and concrete is considered only at the ends of the member. For numerical integration, a member end section is

subdivided as shown in Fig. A3 (c). Stress and strain in each subdivided region are assumed uniform.

(4) Discontinuous cracks due to pull-out of rebars occur only at both ends of the member as shown in Fig. A3 (b). The crack may occur over the total section as shown in Fig. A4.

(5) The concrete strain at the tip of the crack (C_A and C_B in Fig. A3 (b)) is ${}_c\varepsilon_T$, the strain when the concrete loses tensile stress (see Fig. 3).

(6) Concrete strain varies linearly along the member axis as shown in Fig. A3 (a).

(7) After cracking, the steel strain is related to the concrete strain at the end of the elastic region considering the effect of tension stiffening: the relationship is given by that of the equivalent model bar in concrete of length d shown in Fig. A5, where $\bar{\varepsilon}_s$ is the strain of steel at the ends and $\bar{\varepsilon}_c$ is the average strain of concrete including crack openings defined below:

$$\bar{\varepsilon}_c = \frac{\int_0^d \varepsilon_c dx + 2n\bar{s}}{d} \tag{A9}$$

where ε_C is concrete strain, n is the number of cracks which increases as $\bar{\varepsilon}_s$ increases, and $\bar{s}$ is slip at the ends of the concrete. The relationship between $\bar{\varepsilon}_s$ and $\bar{\varepsilon}_c$ is analytically given assuming linear elasticity of steel, concrete and bond ($\sigma_S = E_S\varepsilon_S$, $\sigma_C = E_C\varepsilon_C$ and $\tau = Ks$); considering the tensile strength of the concrete; noting the equilibrium

$$A_sE_s\varepsilon_s + A_cE_c\varepsilon_c = A_sE_s\bar{\varepsilon}_s \tag{A10}$$

where A_S, E_S, and ε_S (or A_C, E_C, and ε_C) are sectional area, Young's modulus, and strain of the steel (or the concrete); and solving Eqs. A7 and A8, which yields a second-order linear differential equation. If bond is stiff (large K), tensile cracks occur profusely and the average concrete strain including the cracks approximates steel strain. If bond is loose (small K), tensile cracks do not occur and the average concrete strain remains small.

(8) The curvature κ and the axial strain ε_O of the member axis is represented by the concrete strains at the top and bottom bars ${}_c\varepsilon_t$ and ${}_c\varepsilon_b$ as shown by the following equation, where ${}_c\varepsilon_t$ and ${}_c\varepsilon_b$ include crack widths c_1 through c_4 at member ends shown in Fig. A1 (a).

$$\kappa = \frac{{}_c\varepsilon_t - {}_c\varepsilon_b}{2g} \tag{A11}$$

where $2g$ is the distance between top and bottom reinforcement.

$$\varepsilon_o = \frac{{}_c\varepsilon_t + {}_c\varepsilon_b}{2} \tag{A12}$$

Concrete strains and crack widths

We denote the concrete strains at the top and bottom bars at the end of a member by the following vector.

$$\varepsilon = \{-{}_c\varepsilon_1, -{}_c\varepsilon_2, {}_c\varepsilon_3, {}_c\varepsilon_4\}^t \tag{A13}$$

Similarly, we denote the crack widths and the steel forces at the same points by the following vectors.

$$c = \{-c_1, -c_2, c_3, c_4\}^t \tag{A14}$$

$$\sigma = \{-A_t\sigma_1, -A_t\sigma_2, A_b\sigma_3, A_b\sigma_4\}^t \tag{A15}$$

where A_t and A_b are the sectional area of top and bottom reinforcement.

Numerically solving Eqs. A7 and A8 under the boundary conditions at the critical sections, the following equation is obtained for the top rebar.

$$\Delta\begin{pmatrix} -{}_c\varepsilon_1 \\ {}_c\varepsilon_3 \\ -c_1 \\ c_3 \end{pmatrix} = \begin{bmatrix} R_1 \\ R_2 \end{bmatrix} \Delta\begin{pmatrix} -A_t\sigma_1 \\ A_b\sigma_3 \end{pmatrix} \tag{A16}$$

A similar equation is obtained for the bottom rebar. Rearranging these equations, the following matrices N_1 and N_2 are obtained between ε, c and σ.

$$\Delta\begin{pmatrix} \varepsilon \\ c \end{pmatrix} = \begin{bmatrix} N_1 \\ N_2 \end{bmatrix} \Delta\sigma \tag{A17}$$

Deformation vector, inner force vector and stiffness matrix

Substituting κ of Eqs. A11 into Eq. A3 and utilizing the Assumption 6, θ_A is obtained as follows.

$$\theta_A = \frac{\ell}{3}\frac{-\varepsilon_{c1} + \varepsilon_{c2}}{2g} + \frac{\ell}{6}\frac{\varepsilon_{c3} - \varepsilon_{c4}}{2g} + \frac{-c_1 + c_2}{2g} \tag{A18}$$

The other components of the deformation vector d can be similarly expressed using ε and c. Thus the following matrices, H_1 and H_2, are obtained.

$$d = [H_1 \quad H_2] \cdot \begin{pmatrix} \varepsilon \\ c \end{pmatrix} \tag{A19}$$

Substituting Eq. A17 into Eq. A19, we have

$$\Delta d = C\,\Delta\sigma \tag{A20}$$

$$\text{where } C = H_1 N_1 + H_2 N_2 \tag{A21}$$

The inner force vector f is decomposed into the contributions by steel and concrete, f_S and f_C as follows.

$$f = f_S + f_C \tag{A22}$$

Since f_S is a linear combination of σ, a matrix G is obtained connecting f_S and σ as follows.

$$f_S = G\,\sigma \tag{A23}$$

On the other hand, f_C is given by integrating the stress distribution of Fig. A3 (e) linked with the strain distribution of Fig. A3 (d). Thus we have matrices Q_1 and Q_2 connecting ε, c and f_C as follows. The components of Q_1 and Q_2 are given integrating instantaneous stiffness of concrete over the member end sections.

$$\Delta f_c = [Q_1 \quad Q_2] \cdot \Delta \begin{pmatrix} \varepsilon \\ c \end{pmatrix} \tag{A24}$$

Substituting Eq. A17 into Eq. A24, we have

$$\Delta f_C = E\,\Delta\sigma \tag{A25}$$

$$\text{where } E = Q_1 R_1 + Q_2 R_2 \tag{A26}$$

Substituting Eqs. A23 and A25 into Eq. A22 and using Eq. A20, the stiffness matrix is given as follows.

$$\Delta f = (E + G)\, C^{-1} \Delta d \tag{A27}$$

The analysis in the paper was done providing incremental deformation angles $\Delta\theta_A = \Delta\theta_B$ and unbalanced axial forces at member ends $\Delta N_A = \Delta N_B$, which is produced during the previous loading step due to non-linearity of constitutive models.

We can extend the method applicable to subassemblages with beam-column joints or to frames noting the continuity of stresses and displacements of longitudinal bars at member ends (Ichinose 1986).

Appendix 2: BOND STRESS NEAR CRITICAL SECTIONS

Bond strength is normally governed by the splitting of the cover as tested by Fujii and Morita (1982). Near critical sections, however, we should consider limitation of bond stress due to inclined cracks as shown in Fig. A6 (b). The free body of PQR of this figure is simplified and shown in Fig. A6 (c). The distance between P and Q is assumed as $j = (7/8)d$

where d is the effective depth. The equilibrium of moments around the point P gives the following equation.

$$\frac{7}{8}d \cdot (T_Q - T_R) = \int_0^x x p_w \sigma b \, dx \qquad \text{(A28)}$$

where T_Q and T_R are tensile forces carried by the longitudinal reinforcement at points Q and R; x is the distance between Q and R; p_W is the shear reinforcement ratio; σ is the tensile stress of the shear reinforcement; and b is the width of the section. Since we consider Eq. A7 (equilibrium between longitudinal stresses of main bars and bond stresses) and $\sigma \leq \sigma_y$ (= yield strength), we have

$$\frac{7}{8}d \cdot \int_0^x \psi\tau \, dx \leq \int_0^x x p_w \sigma_y b \, dx \qquad \text{(A29)}$$

Differentiating the two sides of this equation, we have:

$$\tau < \frac{x\, p_w \sigma_y b}{(7/8) d\, \psi} = \tau_{max} \qquad \text{(A30)}$$

Thus, this is considered the upper limit of the bond strength governed by inclined cracks. This is illustrated in Fig. A6 (a) as τ_{max}. In the region where τ_{max} is smaller than the splitting bond strength, the bond-slip relationship is reduced as shown by the solid line in Fig. A6 (d), where the broken line indicates a model without the reduction.